Measurement and parameterization of albedo variations at Haut Glacier d'Arolla, Switzerland

BEN W. BROCK,[1] IAN C. WILLIS,[2] MARTIN J. SHARP[3]

[1]*Department of Geography, University of Dundee, Dundee DD1 4HN, Scotland*
[2]*Department of Geography, University of Cambridge, Downing Place, Cambridge CB2 3EN, England*
[3]*Department of Earth and Atmospheric Sciences, University of Alberta, Edmonton, Alberta T6G 2E3, Canada*

ABSTRACT. Spatial and temporal variations of surface albedo on Haut Glacier d'Arolla, Switzerland, during the 1993 and 1994 ablation seasons are described. Correlation and regression analyses are used to explain the albedo variations in terms of independent meteorological and surface property variables. Parameterizations are developed which allow estimation of albedo variation in surface energy-balance models. Snow albedo is best estimated from accumulated daily maximum temperatures since snowfall. On "deep" snow (≥ 0.5 cm w.e. depth) a logarithmic function is used, while on "shallow" snow (< 0.5 cm w.e. depth) an exponential function is used to enable the albedo to decay to the underlying ice or debris albedo. The transition from "deep" to "shallow" snow is calculated as a function of decreasing snow depth (combined $r^2 = 0.65$). This new parameterization performs better than earlier schemes because accumulated daily maximum temperatures since snowfall correlate strongly with snow grain-size and impurity concentration, the main physical controls on snow albedo. Ice albedo may be parameterized by its relationship to elevation ($r^2 = 0.28$), but this approach results in only a small improvement over the assumption of a constant mean ice albedo.

1. INTRODUCTION AND AIMS

The surface albedo (α), defined as the broadband hemispherically averaged reflectance in approximately the spectral range 0.3–2.8 μm, controls the net shortwave radiation flux at a glacier surface. Glacier surface melt rates are highly sensitive to α variations, since surface energy balances during the ablation season are commonly dominated by solar radiation receipts (e.g. Röthlisberger and Lang, 1987). Previous studies have demonstrated a large range in glacier α, from < 0.10 for dirty glacier ice to > 0.90 for fresh snow (see summaries in Oerlemans, 1993, table 1; Paterson, 1994, table 4.1; Cutler and Munro, 1996, table 1). Comparatively little is known, however, about the causes of spatial and temporal glacier α variations, and it has thus been difficult to incorporate their effects into numerical surface melt models at the glacier-wide scale (e.g. Arnold and others, 1996).

To address these problems, this study aims to: (i) monitor spatial and temporal α variations across a glacier throughout two ablation seasons; (ii) relate the patterns of α variation to physical control variables (e.g. snow grain-size, snow impurity concentration and debris cover on ice); and (iii) develop parameterizations of α variation in terms of "surrogate" variables (e.g. air temperature and time) which can be used in energy-balance melt models.

2. BACKGROUND

Previous ground-based studies of glacier α have focused either on short-term-variability at a point (e.g. Hubley, 1955; Konzelmann and Ohmura, 1995) or on documenting spatial patterns which are not adequately explained through physical

control variables (Scheibbner and Mahringer, 1968; Van de Wal and others, 1992). Satellite measurements have much potential for monitoring α variations (e.g. Knap and Oerlemans, 1996), although some aspects of the albedo retrieval methodology need to be resolved (Knap and others, 1999). However, explanation of observed α variations in terms of surface or meteorological conditions requires simultaneous ground-based measurements. There is therefore a need for studies which combine systematic measurements of glacier α variations with measurements of meteorological variables and the physical properties of the surface, such as snow grain-size and debris cover.

The theoretical controls on snow albedo (α_s) are well established (Dozier, 1989; Barry, 1996). The models of Warren and Wiscombe (1980) and Wiscombe and Warren (1980) demonstrate that on a pure, deep snowpack, under constant illumination conditions, α_s depends only on the effective grain-size, while light-absorbing impurities (particularly carbon soot) strongly reduce α_s (just $1 \, \text{mg g}^{-1}$ can reduce α_s by 5–15%). Liquid water in snow reduces α_s by increasing the effective grain-size through the formation of grain clusters (Colbeck, 1979). Snow density probably has a negligible effect on α_s, but on thin snow covers α_s can be reduced by absorption of transmitted radiation in an underlying lower α surface (e.g. ice).

The theoretical controls on ice albedo (α_i) are less well understood. Important factors are likely to be light scattering by bubbles and cracks, which increases α_i (Mellor, 1977), and light absorption by surface debris, dust and liquid water in veins, which reduces α_i.

α increases with solar zenith angle (θ), particularly on old snow and wet ice surfaces, due to increasing forward

scattering of radiation, which may be enhanced by diurnal freeze–melt cycles. However, the effects are greatest at high θ, and α varies little when $\theta < 50$ (e.g. Konzelmann and Ohmura, 1995). The increase in α under cloudy conditions, except when θ is large, is well documented (e.g. Carroll and Fitch, 1981).

To calculate α variation accurately in numerical models, parameterizations must be as physically based as possible. However, the variables which physically control spatial and temporal α variations are difficult to incorporate directly into energy-balance models at the glacier-wide scale. Therefore, surrogate variables, which allow calculation of α variation through their correlation with physical factors, must be used in parameterizations. To date, the physical validity of surrogate variables, such as air temperature, accumulated melt and elevation, used in published α parameterizations, has not been established through field measurement. Furthermore, the accuracy of previous parameterizations has rarely been independently verified.

3. MEASUREMENT

Following preliminary fieldwork in September 1992, field data were collected at Haut Glacier d'Arolla, Valais, Switzerland (Fig. 1), between May and September 1993 and during July and August 1994.

Albedo

α was measured with a Kipp and Zonen CM7B albedometer sensitive to radiation in the wavelength range 0.3–2.8 μm.
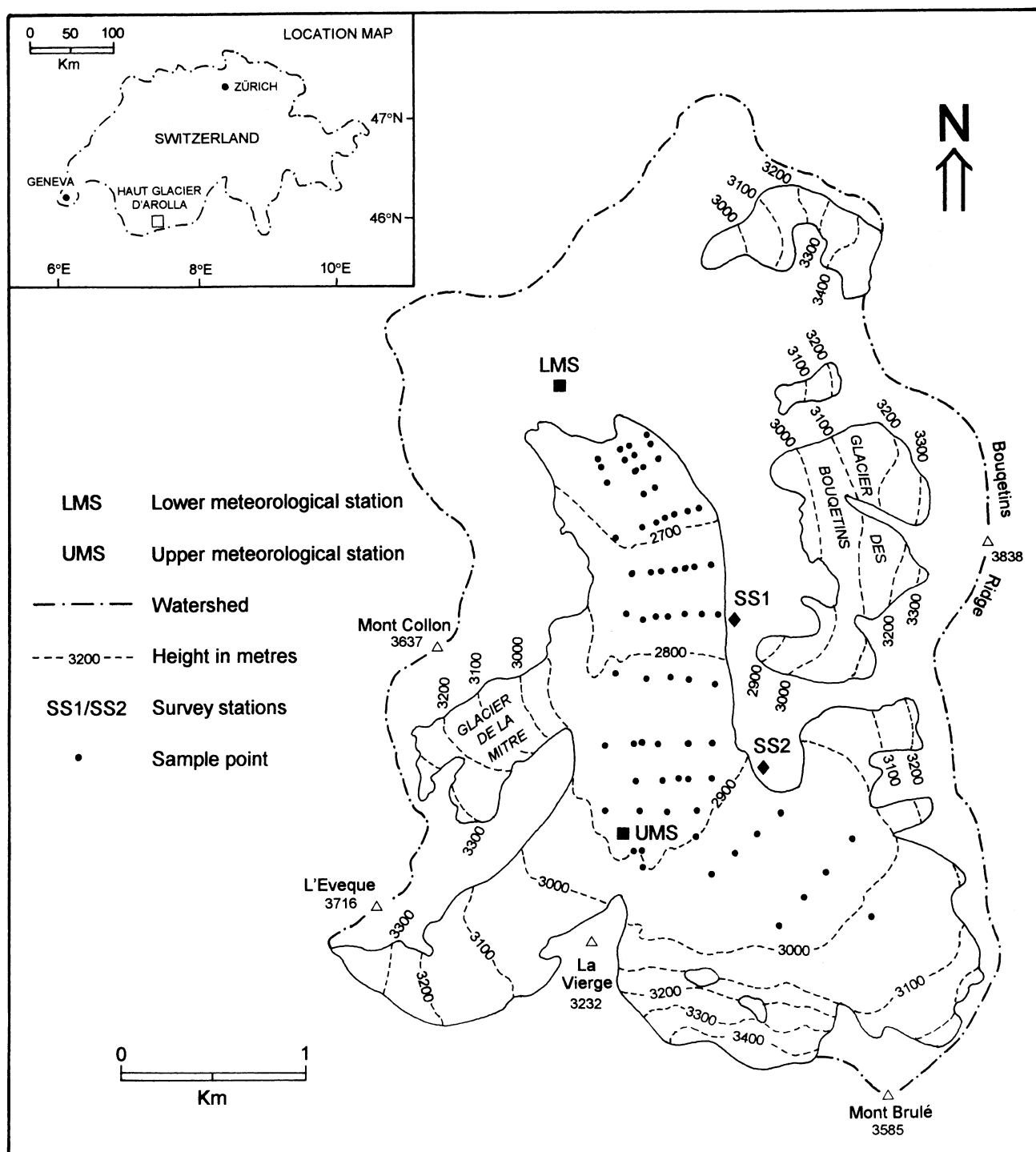

Fig. 1. Site map of Haut Glacier d'Arolla.

The instrument was calibrated by comparison with a reference pyranometer (model: Kipp and Zonen CM6B) using a 1000 W tungsten–halogen lamp. To record spatial variations and seasonal trends in α, rather than α variations caused by changes in cloud cover and θ, the following measurement procedures were used.

1. α was measured under cloud-free conditions within 3 hours of local solar noon, when pyranometer accuracy is $\pm 2\%$. Point α was found to vary by $\leq \pm 0.02$ within this period, irrespective of surface type. Therefore, the influence of varying θ can be ignored in the α measurements. Similarly, the impact of diurnal freeze–melt cycles was avoided since the glacier surface was always melting when measurements were made, except during periods of cold weather when the surface remained frozen throughout the day.

2. The albedometer was mounted on a camera tripod to ensure that α readings were made in a surface-parallel plane. This effectively maintained consistent viewing geometry between different sites and avoided the serious errors which may occur when α is measured in a horizontal plane over a sloping surface (Mannstein, 1985).

3. Measurements were made at 1 m above the surface, at which height 90% of the total irradiance recorded by the downfacing pyranometer is received from a circular area with 3 m radius directly beneath it (Schwerdtfeger, 1976).

Surface properties and meteorological variables

To investigate the influence of surface conditions on α variation, the following variables were measured at each snow-covered point, based on the mean of three samples: snow depth (error $= \pm 1\,\mathrm{cm}$); surface snow density (error $= \pm 5$ kg m^{-3}); surface snow grain-size, defined as sphere diameter (error $= \pm 0.1\,\mathrm{mm}$). At 36 sample points the solid impurity content of the surface snow was determined by filtering 500 mL of melted snow, sampled from directly beneath the albedometer, through a $0.7\,\mu m$ millipore filter paper. The weight of solid impurities contained in the snow sample was calculated as the difference in filter paper weight before and after filtering (error $= \pm 2$ parts per million (ppm) by weight). On ice, the percentage cover by debris and fine-grained material, on the surface and within cryoconite holes, was assessed with the aid of a $0.5\,\mathrm{m}^2$ quadrat.

To assess the effects of meteorological conditions on α and to develop α parameterizations, meteorological variables were recorded at an automatic weather station located at a proglacial site 200 m from the glacier snout at 2547 m a.s.l., which operated continuously throughout the fieldwork period (LMS in Fig. 1). An identical meteorological station (UMS in Fig. 1) was located on the glacier at 2884 m a.s.l. in July and August 1993 and 1994 to provide the temperature lapse rate. Air temperature (T) was measured at 2 m height using thermistors housed in unaspirated radiation shields. As with all T measurements, there is the possibility of artificial heating under strong incident radiation conditions. However, due to katabatic effects wind speed tended to be high (2–5 m s^{-1}) when global radiation was > 700 W m^{-2}, and the likely T overestimate is ≤ 0.5 K (manufacturer's figure). To determine the relationship of α to accumulated melt, regular measurements of surface lowering were made at ablation stakes at 16 sample points along the glacier centre line.

Sampling strategy

To determine glacier-wide variations in α and surface conditions, 68 sample points, ranging in elevation from 2572 to 3002 m a.s.l., were established (Fig. 1). Above 3000 m a.s.l., measurements could not be made safely due to the hazards of steep slopes and crevasses. No measurements were made on the western margin of the glacier tongue, which is entirely debris-covered. The spacing of sample points was varied from about 200 m in the upper basin to about 50 m on the snout to accommodate the greater α variability at low elevations. Sample point locations were surveyed onto the Swiss grid using a Geodimeter 400 total station.

The entire network was sampled at 2–3 week intervals throughout the 1993 ablation season. All points were normally sampled within a 2–3 day snowfall-free period, producing an almost instantaneous picture of the distribution of α across the glacier surface (Table 1). The proportion of sample points monitored increased during the ablation season as the variability in surface conditions increased. To enable the broad patterns of α variation during 1993 to be compared with those during a second ablation season, with different meteorological and surface conditions, two glacier-wide surveys were also conducted during the 1994 ablation season (Table 1). Prior to glacier surveys 2 and 4, measurements were also made between sample points, to assess small-scale α variability. To study the impact of new snowfalls on α, additional point measurements were made on the days following summer snowfalls on 3 September 1992 and 21 May, 3 and 13 June, and 28 August 1993.

4. ALBEDO VARIATIONS

α variations were interpolated across the glacier from the sample point measurements, for each 1993 glacier survey (Fig. 2). Interpolation was performed using a "fault" interpolation routine, based on a bilinear distance function, which did not alter the original α values (UNIRAS, 1990). The maps were extended to the unsampled and permanently snow-covered regions of the upper accumulation area by estimating α from the snow-surface age, using the relationship established by U.S. Army Corps of Engineers (1956). The western tributary glaciers, not covered by the surveys, were not mapped. The main patterns of α variation which emerge are:

1. Low spatial α variability at the start of the ablation season (Fig. 2a) evolved to strong variability, particularly during

Table 1. Dates and number of points sampled in 1993 and 1994 glacier surveys

Glacier survey	Dates	n		
		Total	Snow	Ice
1	26 and 29 May 1993	29	29	0
2[*]	9 June 1993	14	14	0
3	24 and 25 June 1993	51	47	4
4	8 and 9 July 1993	53	31	22
5	26 and 28 July 1993	61	20	41
6	16–18 August 1993	68	2	66
7	5–7 September 1993	68	49	19
8	25–27 July 1994	32	7	25
9	15 and 16 August 1994	33	1	32

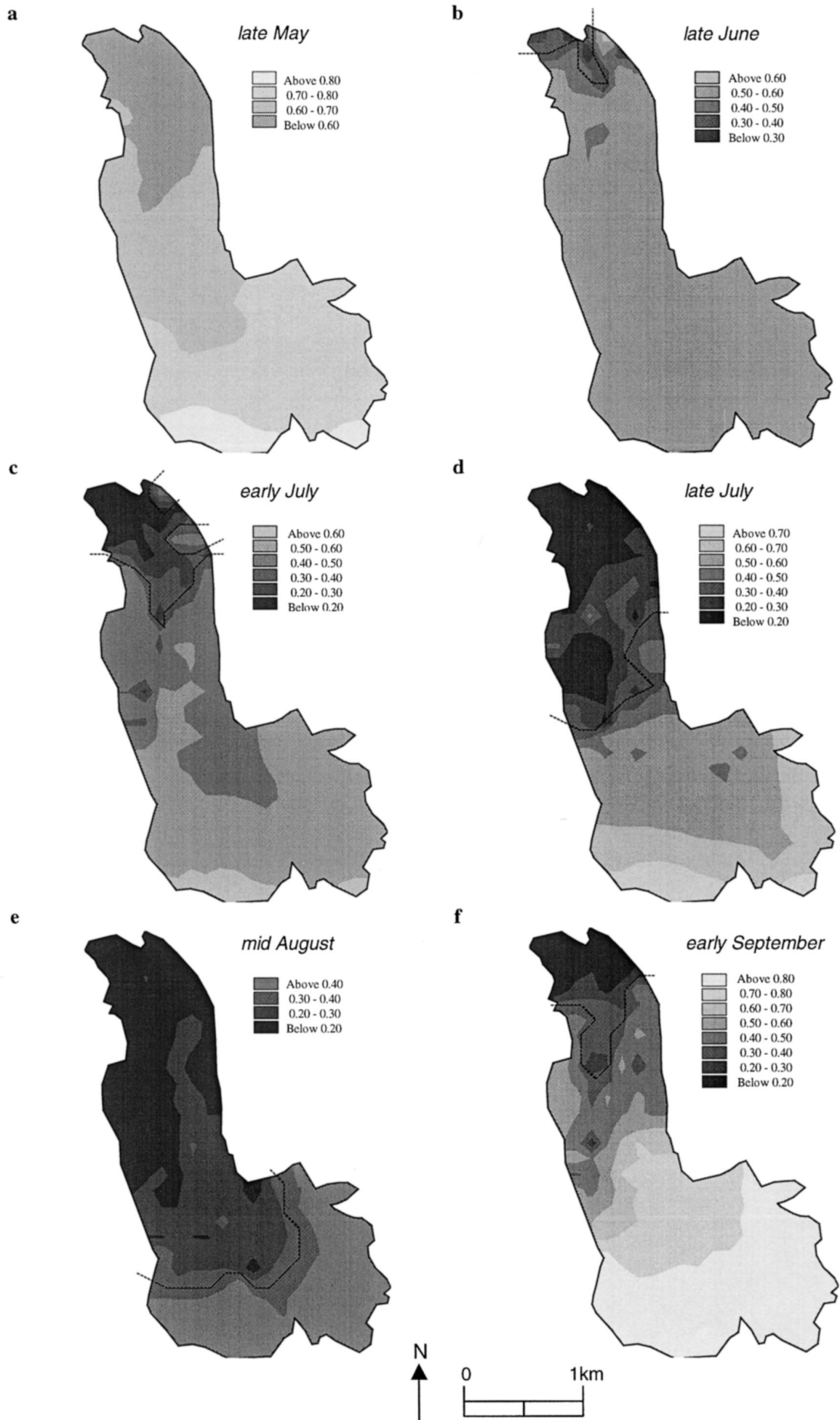[*]Survey 2 had to be abandoned due to bad weather.

Fig. 2. Maps of albedo variation across Haut Glacier d'Arolla in (a) late May, (b) late June, (c) early July, (d) late July, (e) mid-August and (f) early September 1993. The dashed line marks the approximate position of the transient snowline.

July (Fig. 2c–d) and early September (Fig. 2f). The associated increase in α range (Fig. 3a–f) resulted from the transition from a complete glacier-wide snow cover to a mixture of surface types, including snow at differing stages of metamorphism and ice with varying debris cover.

2. α generally increased up-glacier, although only during late May and early September 1993 was there a strong increase with elevation on snow (Figs 2a–f and 4a–c). Below the snowline, the increase in α_i up-glacier was erratic during July and August, with no overall increase apparent in August 1994 (Fig. 4b and c).

3. Early in the ablation season, when α_s was relatively high and the snowline was located close to the glacier snout where α_i was lowest, the α gradient across the snowline was very steep (Figs 2b and c and 4a). It was less steep in August, when α_s was < 0.50 (Figs 2e and 4b).

4. During the mid-ablation season, α varied laterally across the glacier tongue. This was due to faster snowline retreat on the western side of the tongue (July 1993) (Fig. 2c and d) and to higher α_i on the middle and eastern side of the tongue (August 1993) (Fig. 2e).

5. α_s decreased from about 0.80 in late May to 0.40–0.60 during July and August, characteristic of melting snow containing impurities (Fig. 3a–h).

6. The up-glacier retreat of the snowline resulted in a large decrease in point α (Fig. 4a and b). No firn was found due to the lower equilibrium line in 1993 and 1994 compared with previous years.
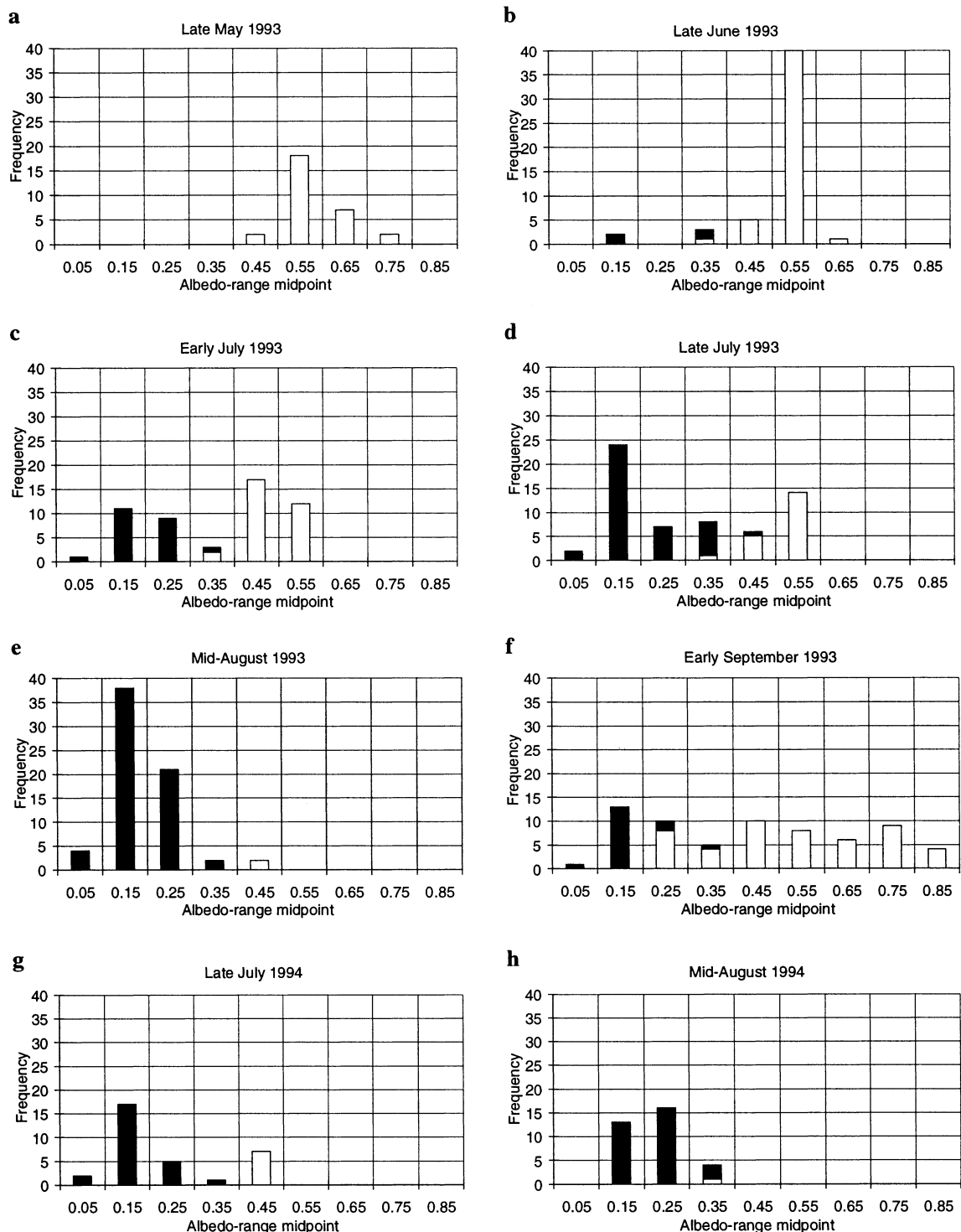

Fig. 3 (a–h). Frequency distributions of sample point albedos during each survey. Black = ice, white = snow. Bin size = 0.10.
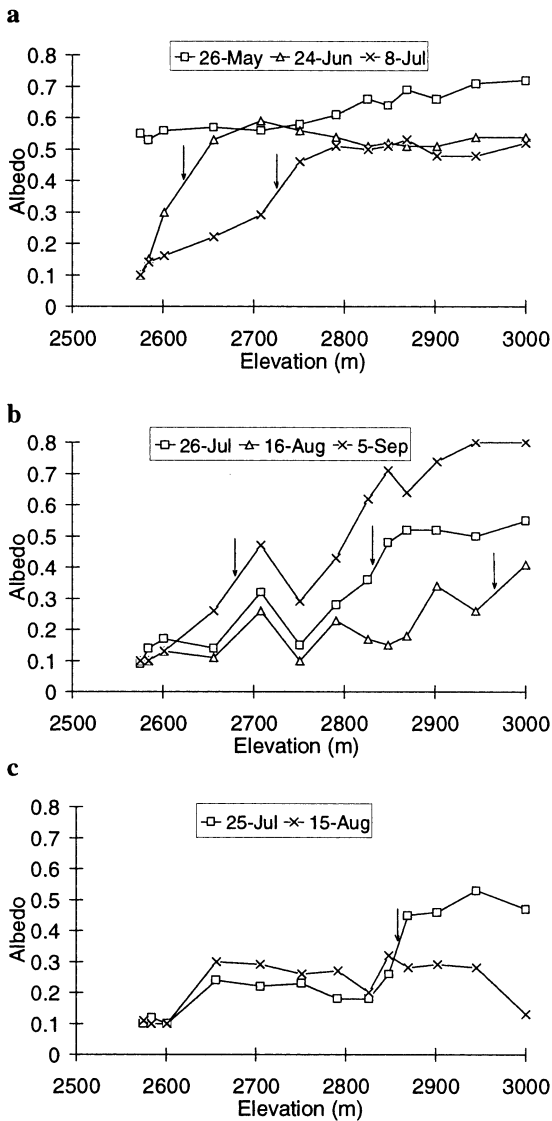
Fig. 4. Albedo along the centre-line profile during the (a, b) 1993 and (c) 1994 ablation seasons. The arrows mark the approximate position of the snowline on each profile.

7. Fresh snowfalls increased α_s to about 0.80 (e.g. between the August and September 1993 surveys; Figs 2e and f and 3e and f), but α_s decreased rapidly to that of the underlying old snow or ice α within a few days of the snowfall (Fig. 5a and b).

8. There was a *decrease* in α_i, of about 0.10 during July and August 1993 (Figs 2d and e, 3d and e and 4a and b). In contrast, α_i *increased*, by a similar amount, over the same period in 1994 (Figs 3g and h and 4c).
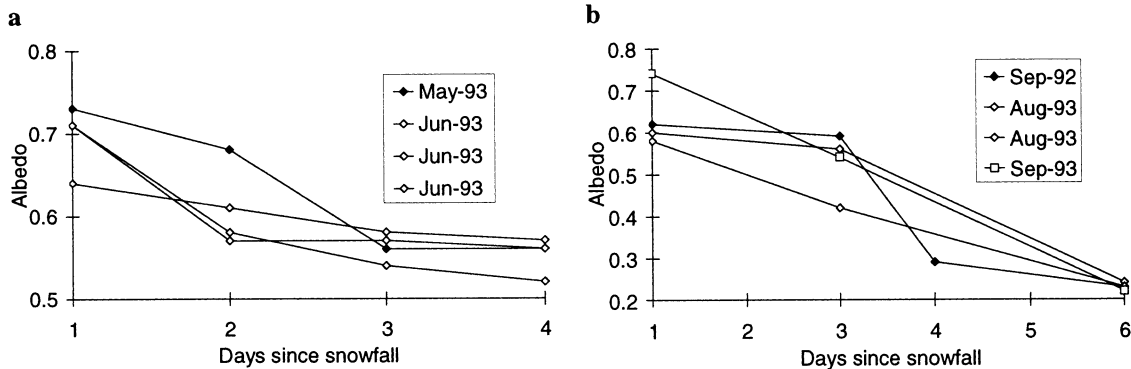
9. Very low values of α_s (<0.40) (e.g. September 1993; Figs 2f and 3f) were associated with thin, patchy snow cover and old snow with high impurity load.

10. Above the snowline, the small-scale α_s variability was generally low (Fig. 2a–d). In the vicinity of the snowline, however, α variability was complex due to the juxtaposition of clean unsaturated snow, dirty saturated snow, ice and debris, and the presence of remnant snow patches below the mean transient snowline (Fig. 2b–e). α_i variability was also spatially complex (e.g. Figs 2d–f and 4b and c), due particularly to variable debris cover at a spatial scale of tens of metres. Very high α variability resulted from a snowstorm on 4 September 1993. At elevations above 2650 m this storm deposited fresh snow ranging in thickness from a thin and patchy cover on the lower tongue to a continuous blanket, with a mean depth of 10 cm, in the upper basin (Fig. 2f). The highest variability occurred at low elevations where the fresh snow cover was discontinuous.

5. ALBEDO VARIABILITY: EXPLANATION AND PARAMETERIZATION

The independent variables used to explain α variability are defined in Table 2.

Relationship of albedo to physical control variables

α_s is inversely correlated with snow grain-size (γ) and impurity concentration (I) (Table 3; Fig. 6a and b) ($r^2 = 0.46$ and 0.74, respectively). Hence, changes in γ and I cause most of the observed α_s variability. α_i is inversely correlated with debris cover (D) (Table 4; Fig. 7a) ($r^2 = 0.41$). This is expected since rock material, dust, carbon soot and organic matter all have lower α than pure ice. Values of $\alpha_i > 0.30$ occurred only when D was $<5\%$.

Parameterization of albedo

Previously published forms of the relationship between α and surrogate variables are shown in Table 5 (referred to as parameterizations A–F hereafter). In these parameterizations, accumulated days (t_a), accumulated daily maximum temperatures $>0°C$ (T_a) and accumulated melt (M_a) (each of which accumulates from a value of zero at the time of the most recent snowfall), snow density (ρ) and snow depth (d) are assumed to be surrogates for increases in γ and I as the snowpack ages. Hence, all parameterizations except A attempt to calculate temporal α_s variability. Parameterizations C–F also aim to calculate spatial α_s variability through

Fig. 5. Change in albedo following fresh snowfall on (a) old snow surfaces, and (b) ice surfaces.

Table 2. Independent variables used to explain albedo variation

	Symbol	Variable	p or s
Snow	γ	Snow grain-size (mm)	p
	I	Snow impurity concentration (ppm)	p
	ρ	Snow density (kg m^{-3})	s
	d	Snow depth (m)	s
	M_a	Accumulated melt since snowfall (m w.e.)	s
	t_a	Accumulated days since snowfall	s
	T_a	Accumulated daily maximum temperatures $> 0°$C since snowfall (K)	s
Ice	D	Debris cover (%)	p
	E	Elevation (m a.s.l.)	s
	M_a	Accumulated melt since exposure of the ice surface (m w.e.)	s
	t_a	Accumulated days since exposure of the ice surface	s

Note: p, physical control variable; s, surrogate variable.

Table 3. Correlation matrix for snow albedo and independent variables

	Albedo (a_s)	Snow grain-size (γ)*	Snow impurity content (I)*
Snow grain-size (γ)*	**−0.679 (177)**		
Snow impurity content (I)*	**−0.862 (34)**	**0.419 (34)**	
Snow density (ρ)	**−0.692 (175)**	**0.399 (162)**	**0.512 (31)**
Snow depth (d)	**0.128 (250)**	−0.020 (161)	**−0.377 (31)**
Accumulated days since snowfall (t_a)*	**−0.546 (311)**	**0.483 (177)**	**0.703 (34)**
Accumulated daily T_{max} since snowfall (T_a)*	**−0.557 (285)**	**0.721 (177)**	**0.608 (34)**
Accumulated melt (M_a)*	**−0.394 (84)**	**0.658 (53)**	**0.690 (18)**

Note: Correlations significant at the 0.05 level are shown in bold type, and the degrees of freedom for each correlation are shown in parentheses.
*Normalized prior to the analyses by taking logarithms.

spatial variations in d, ρ, M_a and T_a. Parameterizations C and E assume that the influence of the underlying ice or debris will increase with decreasing snow-cover thickness and hence α_s will approach the underlying α_i as d decreases.

In parameterization E, α_i decreases as a function of accumulated melt since exposure of the ice surface (M_a), assumed to be a surrogate for increases in D during the ablation season. Similarly, a decrease in α_i over time was calculated as a function of accumulated days since exposure of the ice surface (t_a) using parameterization B (Oerlemans and Hoogendoorn, l989). Parameterization E also calculates spatial α_i variability as a function of elevation (E), on the assumption that α_i will increase up-glacier with decreasing D. The remaining parameterizations do not calculate spatial α_i variability. Only

Table 4. Correlation matrix for ice albedo and independent variables

Variable	Ice albedo (α_i)	% debris cover (D)
% debris cover (D)	**−0.640 (68)**	
Elevation (E)	**0.426 (251)**	−0.063 (67)
Accumulated days (t_a)	**−0.276 (251)**	**0.433 (67)**
Accumulated melt (M_a)	**−0.234 (88)**	**0.783 (15)**

Note: Correlations significant at the 0.05 level are shown in bold type, and the degrees of freedom for each correlation are shown in parentheses.

parameterization D attempts to account for α variability at time-scales of < 1 day.

The validity of the assumptions made by the earlier parameterizations can be tested with the field data. On snow, all surrogate variables used by the parameterizations are significantly correlated with α_s, γ and I, except for d, which is significantly correlated with α_s and I, but not γ (Table 3). The correlations with ρ, T_a and t_a are particularly strong taking sample size into account. Hence, parameterization forms B, D and F have a strong physical basis. However, the occurrence of low α_s (≤ 0.40), causes scatter in the relationships of α_s with surrogate variables (Fig. 6d–g) (snow samples taken for the measurement of ρ required a snow thickness of ≥ 0.1 m, so few values < 0.40 appear in Figure 6c). The assumption that α_s approaches α_i at low values of d (parameterizations C and E) is unsupported (Fig. 6d). As d decreases, α_s becomes increasingly scattered, with a range from < 0.20 to 0.80 occurring when $d < 0.1$ m, compared with the total α_i range of 0.07–0.39. This suggests that variability in γ and I, rather than in α_i, causes most of the scatter in α_s at low values of d.

To determine whether the value of α_s is dependent on the underlying ice or debris albedo (a_u) at very low values of d, correlations between α_s and a_u, for a sample of 54 albedo measurements over shallow snow covers ($d \leq 2$ cm w.e. depth) at which a_u is known, are shown in Table 6. All of the depth ranges in Table 6 include both light deposits of fresh snow and the last remnants of older snow overlying the ice. Measurements of γ and I are not available for most of these points. Instead, correlations of α_s with T_a, α_s proxy for snow metamorphism and accumulation of impurities, are shown. Snow covers of < 0.5 cm w.e. depth were discontinuous, with bare patches of the underlying ice or debris exposed within the field of view of the albedometer.

The most striking result is that α_s is significantly correlated with a_u only on snow < 0.5 cm w.e. deep (Table 6). α_s and a_u are not correlated on deeper snow, despite the large range in a_u. Therefore, snow metamorphism and accumulation of impurities control α_s variability on snow > 0.5 cm w.e. deep, as demonstrated by the very strong inverse correlation between α_s and T_a and by the very large range in α_s (Table 6). Furthermore, α_s is as strongly correlated with T_a as with a_u on snow covers < 0.5 cm w.e. deep, where the α_s range is 0.20–0.68. This implies that a light dusting of fresh snow on an ice or debris surface will dramatically increase the albedo to as high as 0.68, indicating that α_s is virtually independent of a_u. By contrast, the last remnants of an old snowpack lying on top of the ice will have an α_s value similar to that of the underlying ice or debris, due partly to the low α_s of the snow itself and partly to the influence of a_u. An important implication is that α_s will not necessarily approach a_u with decreasing d. Rather, for fresh snow the transition from high α_s to low a_u will occur extremely rapidly when d decreases below 0.5 cm w.e. On old snow, however, the transition to the value of a_u will occur largely as a result of increases in γ and I during snow metamorphism, with a_u an additional factor playing a role only briefly before the snow melts away completely.

On ice, the assumption that t_a and M_a are surrogates for increases in D over the ablation season (parameterizations B and E) has some support from the correlation analysis, but t_a and M_a are weakly correlated with α_i (Table 4; Fig. 7c and d). Of the surrogate variables, E is most strongly correlated with α_i (Table 4; Fig. 7b), although this cannot be explained
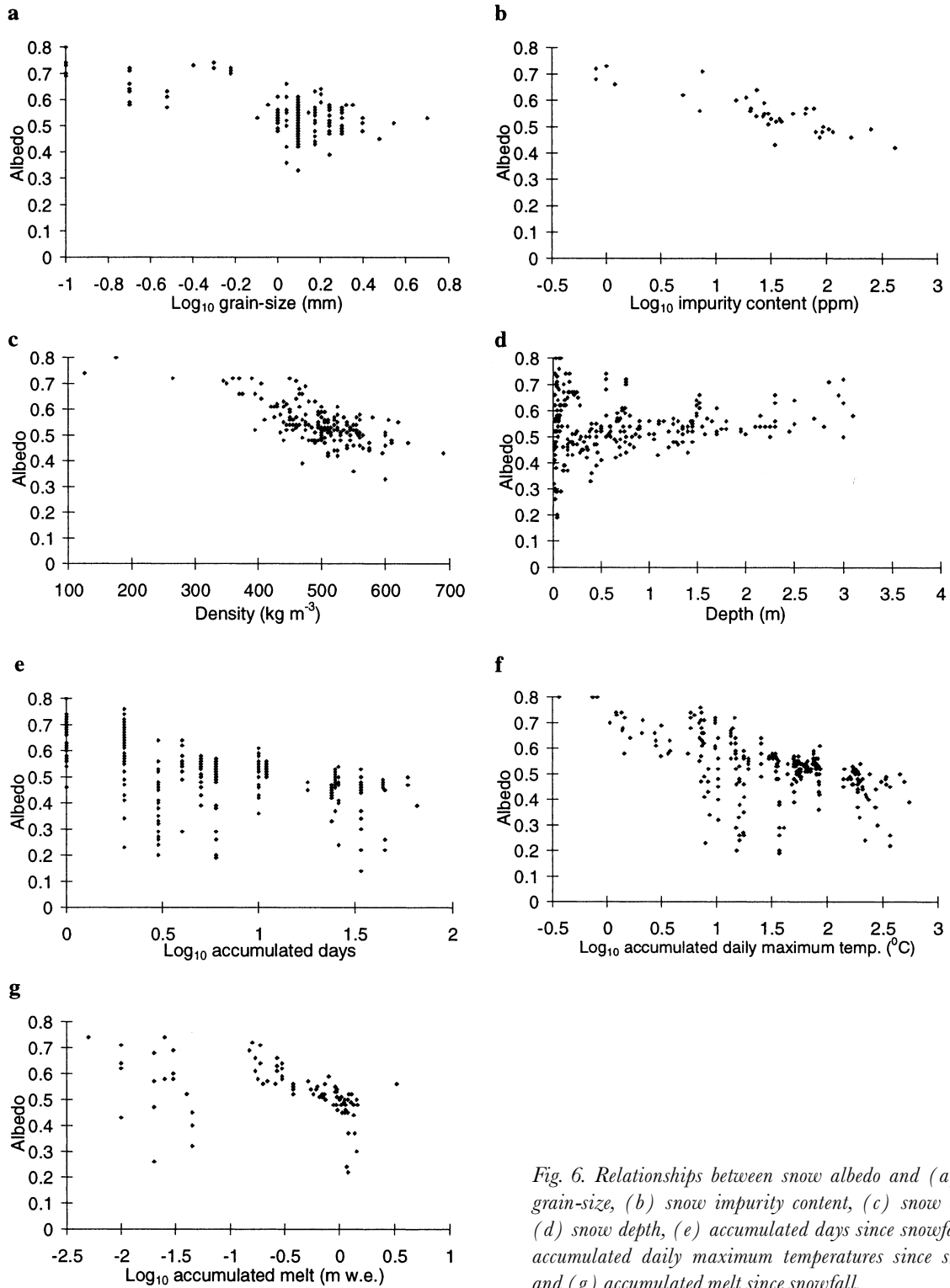
681

Fig. 6. Relationships between snow albedo and (a) snow grain-size, (b) snow impurity content, (c) snow density, (d) snow depth, (e) accumulated days since snowfall, (f) accumulated daily maximum temperatures since snowfall and (g) accumulated melt since snowfall.

through a longitudinal trend in D, as assumed in parameterization E, since E and D are not significantly correlated (Table 4). This may be because of longitudinal variability in air-bubble and crack density, which were not recorded.

Development of new parameterizations: snow albedo

A new α_s parameterization is proposed which differs from previous schemes in form and in the treatment of shallow snow covers.

1. In previous work, α_s is calculated as an exponential function of t_a, T_a or d (Table 5). Hence, following snowfall, the calculated α_s decays rapidly to a constant and is invariable on snow > 10 days old (e.g. Tangborn, 1984) (although parameterization E allows for further decrease in α_s with in-

creasing M_a). In reality, however, α_s decreases gradually for several weeks after snowfall (Fig. 6e–g). This may be attributed to increasing I in the snowpack. Therefore, it is more realistic to calculate α_s from a logarithmic relationship in which the initial rapid α_s decrease following snowfall becomes more gradual over time, without reaching a constant minimum value:

$$\alpha_s = p_1 - p_2 \log S, \qquad (1)$$

where p_1 is the fresh snow α, p_2 is a parameter and S is a surrogate variable.

2. In contrast to earlier work, which relates α_s to a_u as a function of decreasing d, the relationship of α_s to a_u on shallow snow covers ($d < 0.5$ cm w.e.) must be param-
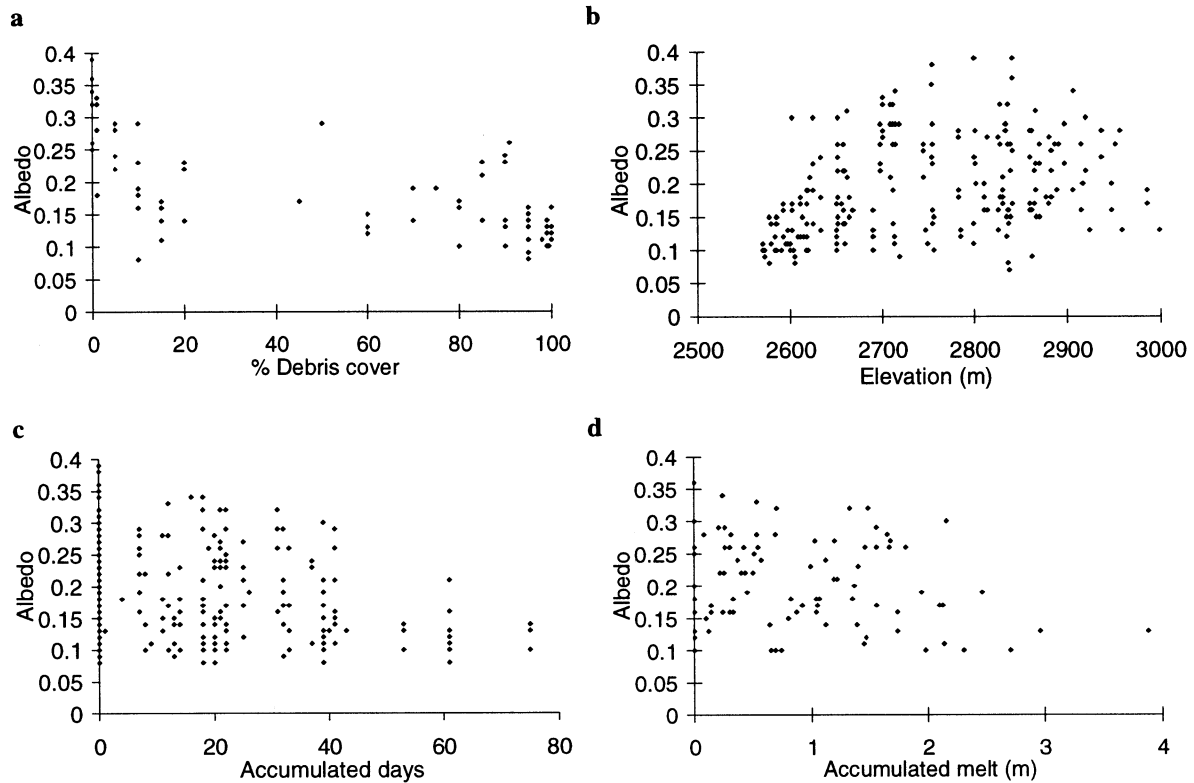
Fig. 7. Relationships between ice albedo and (a) % debris cover, (b) elevation, (c) accumulated days since ice exposure and (d) accumulated melt since ice exposure.

eterized using surrogate variables which correlate with γ and I, to calculate high values of α_s when the snow is fresh and a transition to a_u as the snow metamorphoses.

Taking the above points into account, the best α_s parameterization was identified from least-squares regression ana-

lyses between α_s and all the surrogate variables, using linear, logarithmic and exponential models. The analysis was conducted first for deep snow ≥ 0.5 cm w.e. deep (α_{ds}), and second for shallow snow < 0.5 cm w.e. deep (α_{ss}). The largest amount of α_{ds} variability is explained by a logarithmic relationship to T_a. Additional surrogate variables either

Table 5. Possible forms of albedo parameterization

Parameterization Type[Author]	Independent variables	Form
A "constant albedo"[1-4]	–	Constant α for different surface types (e.g. snow/ice/slush/firn)
B "snow age"[5-8]	t_a	$\alpha_s = p_1 + p_2\,e^{-t_a p_3}$; p_1 to p_3 are parameters
C "snow age and depth"[9]	t_a, d	$\alpha = \alpha_s + \alpha_i - \alpha_s\,e^{(-d/d^*)}$, where: $\alpha_s = \alpha_{firn} + (\alpha_{frsnow} - \alpha_{firn})\,e^{(-t_a/t^*)}$ α_{firn}, α_{frsnow} are characteristic firn and fresh snow α; d^* and t^* are scaling lengths for d and t_a, respectively
D "density, melt rate, solar angle and cloud cover"[10, 11]	ρ	$\alpha = p_1 - p_2\rho_0 + p_3\,e^{(-m/0.5)} + p_4 n + p_5(p_6 - p_7\cos(\theta))(1-n)$ ρ_0 is snow, firn or ice density, m is the surface melt rate, θ is solar zenith angle, n is cloud cover (0.0–1.0), p_1 to p_7 are parameters
E "snow depth, accumulated melt and elevation"[12, 13]	d, M_a, E	$\alpha = \max[0.12, \alpha_{frsnow} - (\alpha_{frsnow} - \alpha_b)\,e^{-p_1 d} - p_2 M_a]$, where α_{frsnow} is the characteristic α of "fresh snow"; α_b, the "background α profile", is: $\alpha_b = p_3\tan^{-1}[(E - L + p_4)/p_5] + p_6$ $L =$ equilibrium-line altitude, p_1 to p_6 are parameters
[14]		New snow up to 3 days old (α_{new}) is calculated from: $\alpha_{new} = \alpha_{ns} - (\alpha_{ns} - \alpha')\,e^{-5000 f}$ α_{ns} is characteristic α of new snow, α' is snow or ice α prior to the new snowfall, f is fresh snow depth in m w.e.
F "exponential function of temperature"[15]	T_a	$\alpha_s = p_1 + p_2\,e^{-T_a p_3}$; p_1 to p_3 are parameters (α_s has also been parameterized as a linear function of T_a [16])

[1]Escher-Vetter (1980); [2]Braithwaite and Olesen (1990); [3]Munro (1991); [4]Hock and Noetzli (1997); [5]U.S. Army Corps of Engineers (1956); [6]Tangborn (1984); [7]Oerlemans and Hoogendoorn (1989); [8]Plüss and Mazzoni (1994); [9]Oerlemans and Knap (1998); [10]Greuell and Oerlemans (1986); [11]Greuell and Konzelmann (1994); [12]Oerlemans (1992); [13]Oerlemans (1993); [14]Arnold and others (1996); [15]Ranzi and Rossi (1991); [16]Winther (1993).
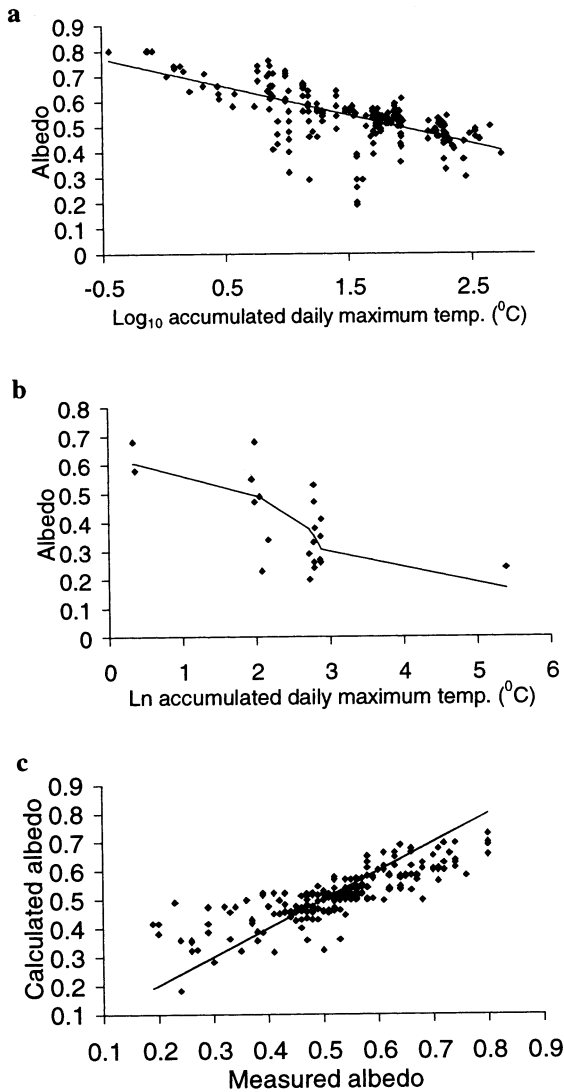
a

b

c

Fig. 8. (a) Variation in measured albedo over deep snow (symbols) and albedo calculated from Equation (2) (solid line). (b) Variation in measured albedo over shallow snow (symbols) and albedo calculated from Equation (3) (solid line). (c) Comparison of measured snow albedo and albedo calculated from Equation (4). The straight line indicates a 1:1 relationship.

violate colinearity or result in no significant increase in r^2 (Table 7):

snow depth ≥ 0.5 cm w.e.:

$$\alpha_{ds} = 0.713 - 0.112 \log_{10} T_a . \tag{2}$$
$$\phantom{\alpha_{ds} = 0.}{(0.0137)} \quad {(0.0083)}$$

(The standard error of each regression coefficient is shown in parentheses.)

In Equation (2), α_{ds} decreases from 0.71 when $T_a = 1$ to 0.50 when $T_a = 80$ (Fig. 8a), but further decay in α_{ds} is very gradual. For example, $\alpha_{ds} = 0.40$ is reached only at $T_a = 623$. Values > 0.71 are calculated when T_a is 0.0–1.0.

The largest amount of α_{ss} variability is explained through an exponential relationship to T_a (Table 7):

snow depth < 0.5 cm w.e.:

$$\alpha_{ss} = a_u + 0.442\, e^{(-0.058 T_a)} . \tag{3}$$
$$\phantom{\alpha_{ss} = }{(0.0537)}\,{(0.0118)}$$

When $T_a = 1$, calculated α_{ss} is equal to a_u plus 0.42, but α_{ss}

Table 6. Correlation of snow albedo (a_s) with the underlying ice or debris albedo (a_u) and accumulated daily maximum temperatures since snowfall (T_a) for shallow snow covers

Snow depth (w.e.)	a_u	$\log_{10} T_a$	a_u range	α_s range
< 0.5 cm, $n = 21$ (21)	**0.641**	**−0.637**	0.09–0.29	0.20–0.68
$\geq 0.5 \leq 1$ cm, $n = 16$ (14)	−0.02	**−0.716**	0.07–0.27	0.26–0.74
> 1 cm ≤ 2 cm, $n = 17$ (13)	0.154	**−0.848**	0.10–0.34	0.20–0.73
$\geq 0.5 \leq 2$ cm, $n = 33$ (27)	0.091	**−0.782**	0.07–0.34	0.20–0.74

Note: n is the sample size for a_u (n) is the sample size for T_a. Numbers in roman font are Pearson's correlation coefficients. Correlations significant at the 0.05 level are shown in bold type.

Table 7. Summary statistics for snow and ice albedo equations developed in this paper

Equation	Dependent variable	r^2	F-ratio	P	n
2	α_{ds}	0.438	184	99.99	236
3	α_{ss}	0.765	325	99.99	21
4	α_s	0.648	543	99.99	257
5	α_i	0.284	51	99.99	253

Note: P is the confidence level at which F is significant; n is the sample size.

decays rapidly to a_u as the snow metamorphoses, and is equal to $a_u + 0.01$ when $T_a = 65$ (Fig. 8b).

There is discontinuity between Equations (2) and (3) for a snowpack melting down on top of the ice. For example, at $T_a = 100$, α_s will jump from 0.49 (Equation (2)) to a_u (Equation (3)) when $d < 0.5$ cm w.e. This is overcome through a transition from α_{ds} to α_{ss} as a function of decreasing d:

$$\alpha_s = (1 - e^{-d/d^*})\alpha_{ds} + e^{-d/d^*}\alpha_{ss} , \tag{4}$$

where d^* is a scaling length for d, which was found by optimization to be equal to 2.4 cm w.e. Hence, for $d > 5$ cm w.e., α_{ss} has negligible influence on α_s. When $d = 1.7$ cm w.e. α_{ds} and α_{ss} make equal contributions to α_s, and when $d < 1.0$ cm w.e. α_s is dominated by α_{ss}. Equation (4) results in a successful parameterization of α_s variability (Table 7). In general, calculated α_s matches measured α_s well (Fig. 8c). The main problems are a tendency to underestimate the high α_s and to overestimate low α_s.

Generally, α_s values calculated from earlier parameterizations must be constrained to ensure that unrealistic values are not calculated when applied outside of the calibration range. Similarly, when $T_a \leq 0$, no solution to Equation (2) can be found and α_s values > 1.0 may be calculated by Equation (3). Additionally, $\alpha_s > 1.0$ will be calculated by Equation (2) when T_a is very small (e.g. 0.001). Therefore, α_s values calculated from Equations (2–4) should be constrained below an upper limit of 0.85 (the highest α_s recorded), which can be achieved simply in a numerical model.

Development of new parameterizations: ice albedo

The best α_i parameterization was identified through regression between α_i and the surrogate variables using a stepwise least-squares procedure, applying linear and polynomial models. Neither t_a nor M_a accounted for a significant amount

of α_i variability. α_i is best parameterized through a second-order polynomial based on elevation (E) (Fig. 9a):

$$\alpha_i = (490.88 - 0.34372E + 6.077 \times 10^{-5}E^2)^{-1} \quad (r^2 = 0.28).$$
$$\qquad\quad (87.0) \qquad (0.06340) \qquad (1.153 \times 10^{-5}) \qquad\qquad (5)$$

The correspondence between measured and calculated α_i is moderate, as only longitudinal α_i variation, not cross-glacier or temporal variation, is calculated (Table 7; Fig. 9b).

Comparison between albedo parameterizations

The performances of the new α parameterizations (Equations (4) and (5), referred to as parameterization G in this subsection) and previous schemes (Table 5) were compared using a common dataset of α_s and α_i measurements. Half of these data were selected randomly for use as a calibration dataset, from which optimal parameter values for each parameterization were obtained. Parameterization performance was assessed on the basis of the accuracy (as expressed by the r^2 and rms error) with which the remaining α values were calculated (the test dataset). Separate calibration and test datasets ensure an impartial comparison of the different schemes. On snow, a dataset of 60 α_s measurements which contained values of all surrogate variables required by the different parameterizations was used initially (Table 8a). However, this dataset contained no measurements on shallow snow, as ρ and M_a (required by parameterizations D and E; Table 5) were generally measured only for deep snow covers. Therefore, the other parameterizations (A, B, C, F and G) were also tested using a larger dataset of 276 α_s measurements from both deep and shallow snow covers, which contained only the required values of t_a, d and T_a (Table 8b). The a_u values required by parameterizations C and G were calculated from Equation (5). On ice, the parameterizations were calibrated and tested using a dataset of 252 α_i measurements, although parameterization E was calibrated and tested using a subset of 90 α_i measurements for which the required M_a values were available (Table 8c). Although not measured specifically, the terms relating to m, θ and n in parameterization D are effectively constants in the Arolla dataset, hence only the term which calculates α_s as a function of ρ was tested.

Results of the comparison: deep snow

All of the parameterizations except A explain a significant amount of α_s variability and have a small rms error (Table 8a). However, parameterization D's performance is relatively poor, suggesting that ρ does not make a good basis for α_s par-

Table 8. Accuracy of albedo parameterizations: summary statistics on (a) deep snow, (b) all snow depths and (c) ice

Parameterization	r^2	rms error	Albedo range	Mean albedo
(a) Snow: deep snow, n = 30				
Measured	–	–	0.46–0.72	0.56
A	0.0	0.07	0.55–0.55	0.55
B	**0.674**	0.04	0.49–0.65	0.55
C	**0.674**	0.04	0.49–0.65	0.55
D	**0.262**	0.06	0.50–0.66	0.56
E	**0.669**	0.04	0.44–0.64	0.56
F	**0.727**	0.04	0.49–0.66	0.55
G	**0.757**	0.03	0.45–0.68	0.55
(b) Snow: all snow depths, n = 138				
Measured	–	–	0.19–0.80	0.52
A	0.0	0.12	0.54–0.54	0.54
B	**0.295**	0.10	0.49–0.80	0.53
C	**0.339**	0.17	0.18–0.92	0.63
F	**0.245**	0.10	0.50–0.77	0.54
G	**0.641**	0.07	0.18–0.76	0.52
*(c) Ice, n = 126 (*n = 45)*				
Measured	–	–	0.08–0.34	0.18
A	0.0	0.07	0.19–0.19	0.19
B	0.015	0.07	0.13–0.19	0.19
C	0.0	0.07	0.19–0.19	0.19
D	0.0	0.07	0.16–0.16	0.16
E*	0.063	0.07	0.15–0.27	0.22
F	0.015	0.07	0.13–0.19	0.19
G	**0.198**	0.06	0.11–0.21	0.17

Note: Bold type indicates a significant r^2 value at the 0.05 significance level. Parameterization G is the new parameterization developed in this paper. n is the sample size.

ameterization. Parameterization E, the most complex scheme tested, performs quite well, but the extra computational effort required is hardly worthwhile when greater accuracy (based on r^2 and rms values) is obtained from simple relationships to T_a (parameterizations F and G) or t_a (parameterizations B and C). Parameterization G has the highest r^2 and lowest rms error of all, and its calculated α_s range corresponds most closely with the measured α_s range. The α_s range calculated by parameterization F is more restricted. This supports the proposal that α_s varies as a logarithmic (i.e. Equation (2)) rather than exponential function (parameterization F) of T_a.

Results of the comparison: all snow depths

The performance of the new scheme (parameterization G) is a dramatic improvement over that of previous schemes
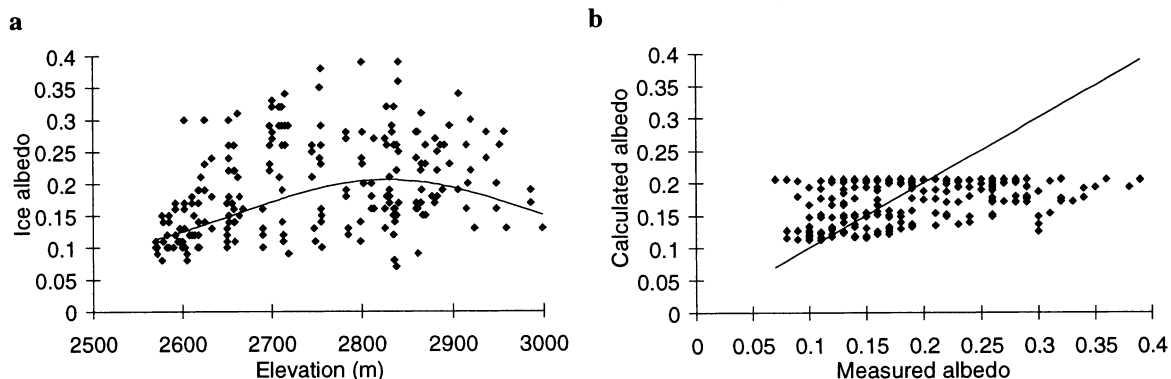

a

b

Fig. 9. (a) Variation in measured ice albedo (symbols) and ice albedo calculated from Equation (5) (line) with elevation. (b) Comparison of measured and calculated ice albedo. The line represents a 1:1 relationship.

685

(Table 8b). The r^2, rms and α_s range statistics demonstrate that Equation (4) successfully calculates both the α_s variation on deep snow and changes associated with the transition to a thin, discontinuous snow cover. By comparison, the performance of the remaining parameterizations is disappointing. The problem of exponential schemes is highlighted by parameterizations B and F. These produce lower α_s limits of 0.49 and 0.50, respectively, leading to an overestimate of low α_s values. Parameterization C, meanwhile, produces a higher rms error than the assumption of a constant mean α_s (parameterization A), and greatly overestimates the mean α_s. These problems occur because this scheme assumes that α_s approaches a_u primarily as a function of d, rather than due to changes to the snowpack during snow metamorphism.

Results of the comparison: ice

Parameterization G is the only one to explain a significant amount of α_i variation and it has the smallest rms error (Table 8c). Parameterization E explains a small amount of α_i variation, but tends to overestimate α_i. Although not specifically developed to calculate α_i variability, the low r^2 values for parameterizations B and F demonstrate the difficulty of calculating temporal α_i variations in terms of t_a and T_a, respectively.

6. DISCUSSION

Physical basis of the new albedo parameterizations

Patterns of α_s variation are dominated by increases in γ and I following snowfall. When $T > 0°C$ this is due mainly to snowmelt, which increases γ through the formation of grain clusters and increases I through snowpack depletion. Thus, T_a is a proxy for the amount of melt, and accounts for both temporal α_s variations and increases in α_s up-glacier, associated with lower melt rates. The logarithmic form of the T_a–α_s relationship (Fig. 8a) results from the combined effects of γ and I. The rapid α_s decay of fresh snow can be attributed to γ growth in approximately the range 10–100 μm, while the accumulation of absorptive impurities causes a more gradual and sustained α_s decrease in older snow as the influence of γ growth diminishes.

The finding that α_s varies independently of a_u on snow covers > 0.5 cm w.e. deep is surprising. This occurs because the influence of a_u on α_s is overwhelmed by the impact of snow metamorphism and the accumulation of impurities. According to theory, the α_s of fresh snow will be independent of a_u, even when d is very small, due to efficient light reflection at the snow surface, but the influence of a_u on α_s will strengthen with the increased forward scattering and penetration of light into the snowpack caused by γ growth (Wiscombe and Warren, 1980). However, it is probable that old snow, which has high concentrations of impurities, is less effective at transmitting light to the underlying ice or debris than theoretical models of pure snow suggest. This explains why α_s and a_u converge on old snow only when $d < 0.5$ cm w.e. depth. However, the scaling depth, d^*, at which the α_s calculation transfers from Equation (2) (independent of a_u) to Equation (3) (dependent on a_u) suggests that a_u does have a small influence in reducing α_s on snow covers up to about 5 cm w.e. deep. The separate parameterization of shallow snow covers enables a much greater amount of α_s varia-

bility to be explained, compared with schemes which treat all snow as independent of a_u. Furthermore, the majority of summer snowfall events, which play a significant role in the surface energy balance, have depths of only a few cm w.e.

Calculation of glacier-wide patterns of α_s using a parameterization based on T_a is dependent on the extrapolation of 2 m T measurements. Normally, this is achieved by assuming a linear lapse rate of 2 m T from a weather station located at a proglacial site, or between two weather stations at differing altitudes. However, the distribution of 2 m temperatures along a glacier is complex, due to the thermal influence of the glacier itself and due to locally strong adiabatic heating of the katabatic wind (e.g. at the base of an icefall). The along-glacier profile of 2 m T is better estimated using a wind model, based on glacier length and slope (Greuell and Böhm, 1998). However, it is useful to consider the error in α_s values calculated from Equation (4) if a standard lapse rate (i.e. 6.5 K km^{-1}) is used to extrapolate 2 m T along-glacier from a proglacial site, as is common procedure in surface energy-balance models. A standard lapse rate may overestimate the true 2 m T by as much as 5 K in warm weather (e.g. a 2 m T in the proglacial area of 288 K) (Van den Broeke, 1997). In this case, the resulting α_s underestimate on deep snow (Equation (2)) is only 0.02 (0.58 instead of 0.60) on the day following a fresh snowfall, and remains 0.02 if 2 m T is overestimated by 5 K on subsequent days. On shallow snow (Equation (3)) the α_s underestimate is 0.06 ($a_u + 0.39$ instead of $a_u + 0.45$) on the day following a fresh snowfall, but reduces to 0.03 if 2 m T is overestimated by 5 K for several days. Therefore, even very large 2 m T errors have a minor impact on α_s estimated using Equation (4). Furthermore, the high temperatures which may result in a large 2 m T overestimate, and a large underestimate of fresh snow α_s in Equation (3), are unlikely to occur immediately after a snowfall.

Comparison of different parameterizations showed that α_s variability may be successfully calculated as a function of t_a. M_a should also be a good predictor of α_s since increases in γ and I are caused by melt. However, M_a correlates with α_s and γ less strongly than T_a does (Table 3). This might be due to errors in converting measurements of surface lowering at ablation stakes into M_a, caused by ρ variation with depth. In any case, M_a makes a poor basis for α_s parameterization in numerical models. First, the accuracy with which M_a values may be estimated across a glacier is subject to errors in the extrapolation of several meteorological and surface (e.g. aerodynamic roughness) variables. Second, the calculation of M_a in an energy-balance model depends on prior knowledge of α_s. Thus, a positive feedback loop may be generated in which an error in the initial α_s estimate would cause an error in the calculation of M_a, which in turn would result in an enlarged α_s error and so on.

A more general problem for surface melt models is the accurate estimation of α in the vicinity of the transient snowline, assuming model gridcells cover areas of > 100 m^2. While, for a given cell, calculated d might be a few cm, in reality the area covered by the cell would be a mosaic of snow patches and bare ice. Hence, α would tend to be overestimated. A possible way to treat this problem is to allow d to vary around the mean from cell to cell to simulate patchy snow cover.

On ice, D accounts for $>40\%$ α_i variability. The remainder is probably caused by variability in air-bubble content and crack density, which are difficult to quantify. α_i was

generally <0.30, lower than the Greenland ice-sheet margin (Konzelmann and Braithwaite, 1995) and Morteratsch-gletscher, Greenland (personal communication from W. H. Knap, 1999), but similar to Hintereisferner, Austria (Van de Wal and others, 1992), and Peyto Glacier, Canada (Cutler and Munro, 1996). This implies that D, air-bubble content and crack density vary between glaciers.

The α_i parameterization, based on E, explains slightly more than a quarter of total α_i variability. Albedo measurements derived from 1993 Landsat imagery of Haut Glacier d'Arolla also demonstrate a weak dependency of α_i on E during August, but the longitudinal α_i variability is less erratic than in Figure 4b and c (Knap and others, 1999). Satellite measurements do not resolve small-scale spatial variability in α_i, but represent the mean α_i over large (e.g. 30 m × 30 m) areas more accurately. The satellite measurements are also able to delineate longitudinal features such as medial moraines and debris bands. As a result, cross-glacier variability appears to be even stronger in the Landsat-derived α_i measurements than in Figure 2d and e. It may therefore be questioned whether Equation (5) is worth the extra computational effort compared with using a constant mean value for α_i, which will suffer from similar magnitude errors.

Parameterization assumptions

Most earlier parameterizations make implicit assumptions about the physical controls on α variation. Some of these assumptions are found to be unsubstantiated when tested with the field measurements collected in this study.

1. The common assumption that α_s systematically approaches a_u with decreasing snow thickness is not substantiated by the field measurements or theory. The effects of metamorphism and accumulation of impurities in the snow dominate over the influence of a_u until the snow cover has all but melted away. Furthermore, d is not significantly correlated with γ, and its correlation with I is weaker than other surrogate variables. Hence, there is little basis for calculating α_s as a function of d, and, when tested with field data, parameterizations based primarily on d are relatively poor at estimating α_s variability.

2. Many previous α_s parameterizations have an exponential form reflecting the behaviour of a pure, deep snowpack. However, this ignores the impact of absorptive impurities, with the result that exponential parameterizations over-estimate α_s on old snow. Exponential forms can be "forced" to calculated lower α_s values, but this seriously diminishes the overall parameterization accuracy.

3. Trends of decreasing α_i over an ablation season are generally assumed to be associated with increasing concentrations of dust and debris on the exposed ice surface (e.g. Oerlemans, 1993). The α_i increase observed between July and August 1994 demonstrates that such trends are not universal. Clearly, there must be additional physical mechanisms which can cause α_i to increase over time, most likely through removal of surface debris by rainfall and runoff. Parameterizations making the assumption that α_i decreases continuously throughout the ablation season will overestimate α_i following an event in which fine debris is washed from the glacier surface.

4. Our measurements do not show the strong dependence of α_i on E which is often assumed. Given the probable differences in D, air-bubble content and crack density between glaciers, universal relationships between α_i and E are unlikely to exist.

7. CONCLUSIONS

This paper presents the first attempt to monitor α variations across a glacier throughout the ablation season and relate them to measurements of surface and meteorological conditions. The main conclusions are:

1. A new parameterization to calculate α_s variability in numerical melt models has been developed, based on separate estimation of α_s on "deep" snow > 0.5 cm w.e. deep, which is independent of a_u, and "shallow" snow < 0.5 cm w.e. deep which becomes dependent on a_u as the snow metamorphoses. The calculation for "deep" α_s transfers to "shallow" α_s an exponential function of decreasing d. This parameterization performs better than previous schemes because T_a, the main predictor variable, correlates strongly with γ and I, which control α_s variability. This parameterization should enable spatial and temporal variations in the net shortwave radiation flux and melt rate across glaciers to be calculated with greater accuracy. Improvements afforded by the new α_i parameterization, based on E, are more modest, reflecting the non-systematic nature of α_i variability.

2. Field measurements are crucial to the development and testing of empirical α parameterizations. Several assumptions about the physical causes of α variation made in earlier parameterizations are found to be unsubstantiated when tested with the field data collected in this study.

3. The α_s parameterization is transferable, but local calibration of the relationship may be necessary due to: (i) variation in I (i.e. α_s will be less sensitive to T_a at unpolluted sites); (ii) differences in the relative contribution of turbulent sensible-heat energy to the surface energy balance, which will affect the relationship of T_a to melt and hence to γ and I.

4. Given the success of satellite-based work in mapping spatial α variability (e.g. Knap and Oerlemans, 1996), remote sensing is the best way to incorporate spatial α_i variability into numerical energy-balance models.

5. The mechanisms which control temporal α_i variation are not well understood and currently cannot be incorporated into numerical melt models. Future studies should aim to quantify: (i) sediment input and dispersal across glaciers; (ii) the mechanisms of fine sediment removal.

6. The parameterizations developed here are valid only for clear-sky conditions and low to medium θ. Further work is needed to extend their applicability by quantifying the effects of clouds and θ variation in terms of variables (e.g. global radiation) which can be incorporated within numerical energy-balance models.

REFERENCES

Arnold, N. S., I. C. Willis, M. J. Sharp, K. S. Richards and W. J. Lawson. 1996. A distributed surface energy-balance model for a small valley glacier. I. Development and testing for Haut Glacier d'Arolla, Valais, Switzerland. *J. Glaciol.*, **42**(140), 77–89.

Barry, R. G. 1996. The parameterization of surface albedo for sea ice and its snow cover. *Prog. Phys. Geogr.*, **20**(1), 63–79.

Braithwaite, R. J. and O. B. Olesen. 1990. A simple energy-balance model to calculate ice ablation at the margin of the Greenland ice sheet. *J. Glaciol.*, **36**(123), 222–228.

Carroll, J. J. and B. W. Fitch. 1981. Effects of solar elevation and cloudiness on snow albedo at the South Pole. *J. Geophys. Res.*, **86**(6), 5271–5276.

Colbeck, S. C. 1979. Grain clusters in wet snow. *J. Colloid Interface Sci.*, **72**(3), 371–384.

Cutler, P. M. and D. S. Munro. 1996. Visible and near-infrared reflectivity during the ablation period on Peyto Glacier, Alberta, Canada. *J. Glaciol.*, **42**(141), 333–340.

Dozier, J. 1989. Remote sensing of snow in visible and near-infrared wavelengths. *In* Asrar, G., *ed. Theory and applications of optical remote sensing*. New York, etc., John Wiley and Sons, 527–547.

Escher-Vetter, H. 1980. Der Strahlungshaushalt des Vernagtferners als Basis der Energiehaushaltsberechnung zur Bestimmung der Schmeltzwasserproduktion eines Alpengletschers. *Universität München. Meteorologisches Institut. Wissenschaftliche Mitteilungen* 39.

Greuell, J. W. and T. Konzelmann. 1994. Numerical modeling of the energy balance and the englacial temperature of the Greenland ice sheet: calculations for the ETH-Camp location (West Greenland, 1155 m a.s.l.). *Global and Planetary Change*, **9**(1–2), 91–114.

Greuell, W. and R. Böhm. 1998. 2 m temperatures along melting mid-latitude glaciers, and implications for the sensitivity of the mass balance to variations in temperature. *J. Glaciol.*, **44**(146), 9–20.

Greuell, W. and J. Oerlemans. 1986. Sensitivity studies with a mass balance model including temperature profile calculations inside the glacier. *Z. Gletscherkd. Glazialgeol.*, **22**(2), 101–124.

Hock, R. and C. Noetzli. 1997. Areal melt and discharge modelling of Storglaciären, Sweden. *Ann. Glaciol.*, **24**, 211–216.

Hubley, R. C. 1955. Measurements of diurnal variations in snow albedo on Lemon Creek Glacier, Alaska. *J. Glaciol.*, **2**(18), 560–563.

Knap, W. H. and J. Oerlemans. 1996. The surface albedo of the Greenland ice sheet: satellite-derived and in situ measurements in the Søndre Strømfjord area during the 1991 melt season. *J. Glaciol.*, **42**(141), 364–374.

Knap, W. H., B. W. Brock, J. Oerlemans and I. C. Willis. 1999. Comparison of Landsat TM-derived and ground-based albedos of Haut Glacier d'Arolla, Switzerland. *Int. J. Remote Sensing*, **20**(17), 3293–3310.

Konzelmann, T. and R. J. Braithwaite. 1995. Variations of ablation, albedo and energy balance at the margin of the Greenland ice sheet, Kronprins Christian Land, eastern north Greenland. *J. Glaciol.*, **41**(137), 174–182.

Konzelmann, T. and A. Ohmura. 1995. Radiative fluxes and their impact on the energy balance of the Greenland ice sheet. *J. Glaciol.*, **41**(139), 490–502.

Mannstein, H. 1985. The interpretation of albedo measurements on a snow covered slope. *Arch. Meteorol. Geophys. Bioklimatol., Ser. B*, **36**, 73–81.

Mellor, M. 1977. Engineering properties of snow. *J. Glaciol.*, **19**(81), 15–66.

Munro, D. S. 1991. A surface energy exchange model of glacier melt and net mass balance. *Int. J. Climatol.*, **11**(6), 689–700.

Oerlemans, J. 1992. Climate sensitivity of glaciers in southern Norway: application of an energy-balance model to Nigardsbreen, Hellstugubreen and Alfotbreen. *J. Glaciol.*, **38**(129), 223–232.

Oerlemans, J. 1993. A model for the surface balance of ice masses: Part 1. Alpine glaciers. *Z. Gletscherkd. Glazialgeol.*, **27–28**, 1991–1992, 63–83.

Oerlemans, J. and N. C. Hoogendoorn. 1989. Mass-balance gradients and climatic change. *J. Glaciol.*, **35**(121), 399–405.

Oerlemans, J. and W. H. Knap. 1998. A 1 year record of global radiation and albedo in the ablation zone of Morteratschgletscher, Switzerland. *J. Glaciol.*, **44**(147), 231–238.

Paterson, W. S. B. 1994. *The physics of glaciers. Third edition.* Oxford, etc., Elsevier.

Plüss, C. and R. Mazzoni. 1994. The role of turbulent heat fluxes in the energy balance of high Alpine snow cover. *Nord. Hydrol.*, **25**(1–2), 25–38.

Ranzi, R. and R. Rossi. 1991. A physically based approach to modelling distributed snowmelt in a small alpine catchment. *International Association of Hydrological Sciences Publication* 205 (Symposium at Vienna 1991 — *Snow, Hydrology and Forests in High Alpine Areas*), 141–152.

Röthlisberger, H. and H. Lang. 1987. Glacial hydrology. *In* Gurnell, A. M. and M. J. Clark, *eds. Glacio-fluvial sediment transfer: an alpine perspective.* Chichester, etc., John Wiley and Sons, 207–284.

Scheibbner, F. and W. Mahringer. 1968. Die Albedo der Sonnblickgletscher und ihre zeitlichen Variationen. *Arch. Meteorol. Geophys. Bioklimatol., Ser. B*, **16**(2–3), 174–194.

Schwerdtfeger, P. 1976. *Physical principles of micrometeorological measurements.* Amsterdam, Elsevier. (Developments in Atmospheric Science 6.)

Tangborn, W. V. 1984. Prediction of glacier derived runoff for hydroelectric development. *Geogr. Ann.*, **66A**(3), 257–265.

UNIRAS. 1990. *Unimap 2000 user's manual. Version 6.* Søborg, Denmark, UNIRAS Ltd.

United States Army Corps of Engineers. 1956. *Snow hydrology: summary report of the snow investigations.* Portland, OR, U.S. Army Corps of Engineers. North Pacific Division.

Van den Broeke, M. R. 1997. Structure and diurnal variation of the atmospheric boundary layer over a mid-latitude glacier in summer. *Boundary-Layer Meteorol.*, **83**, 183–205.

Van de Wal, R. S. W., J. Oerlemans and J. C. van der Hage. 1992. A study of ablation variations on the tongue of Hintereisferner, Austrian Alps. *J. Glaciol.*, **38**(130), 319–324.

Warren, S. G. and W. J. Wiscombe. 1980. A model for the spectral albedo of snow. II. Snow containing atmospheric aerosols. *J. Atmos. Sci.*, **37**(12), 2734–2745.

Winther, J.-G. 1993. Short- and long-term variability of snow albedo. *Nord. Hydrol.*, **24**(2–3), 199–212.

Wiscombe, W. J. and S. G. Warren. 1980. A model for the spectral albedo of snow. I. Pure snow. *J. Atmos. Sci.*, **37**(12), 2712–2733.